10-30-2020

Spiny Mice (*Acomys*) Exhibit Attenuated Hallmarks of Aging and Rapid Cell Turnover after UV Exposure in the Skin Epidermis

Wesley Wong
Northeastern University

Austin Kim
Northeastern University

James R. Monaghan
Northeastern University

Ashley W. Seifert
University of Kentucky, awseifert@uky.edu

Malcolm Maden
University of Florida

See next page for additional authors

Spiny Mice (*Acomys*) Exhibit Attenuated Hallmarks of Aging and Rapid Cell Turnover after UV Exposure in the Skin Epidermis

Digital Object Identifier (DOI)
https://doi.org/10.1371/journal.pone.0241617

Notes/Citation Information
Published in *PLOS ONE*, v. 15, no. 10, e0241617.

Authors
Wesley Wong, Austin Kim, James R. Monaghan, Ashley W. Seifert, Malcolm Maden, and Justin D. Crane

PLOS ONE

RESEARCH ARTICLE

Spiny mice (*Acomys*) exhibit attenuated hallmarks of aging and rapid cell turnover after UV exposure in the skin epidermis

Wesley Wong[1], Austin Kim[1], James R. Monaghan[1], Ashley W. Seifert[2], Malcolm Maden[3], Justin D. Crane[1]*

1 Department of Biology, Northeastern University, Boston, Massachusetts, United States of America, **2** Department of Biology, University of Kentucky, Lexington, Kentucky, United States of America, **3** UF Genetics Institute & Department of Biology, University of Florida, Gainesville, Florida, United States of America

* j.crane@northeastern.edu

Citation: Wong W, Kim A, Monaghan JR, Seifert AW, Maden M, Crane JD (2020) Spiny mice (*Acomys*) exhibit attenuated hallmarks of aging and rapid cell turnover after UV exposure in the skin epidermis. PLoS ONE 15(10): e0241617. https://doi.org/10.1371/journal.pone.0241617

Editor: N. Rajendra Prasad, Annamalai University, INDIA

Received: May 20, 2020

Accepted: October 17, 2020

Published: October 30, 2020

Data Availability Statement: All relevant data are within the manuscript and its Supporting Information files.

Funding: This work was supported by startup funding from the Northeastern University Provost's Office (toJ. D. C.). The funders had no role in study design, data collection and analysis, decision to publish, or preparation of the manuscript.

Competing interests: The authors have declared that no competing interests exist.

Abstract

The study of long-lived and regenerative animal models has revealed diverse protective responses to stressors such as aging and tissue injury. Spiny mice (*Acomys*) are a unique mammalian model of skin wound regeneration, but their response to other types of physiological skin damage has not been investigated. In this study, we examine how spiny mouse skin responds to acute UVB damage or chronological aging compared to non-regenerative C57Bl/6 mice (*M. musculus)*. We find that, compared to *M. musculus*, the skin epidermis in *A. cahirinus* experiences a similar UVB-induced increase in basal cell proliferation but exhibits increased epidermal turnover. Notably, *A. cahirinus* uniquely form a suprabasal layer co-expressing Keratin 14 and Keratin 10 after UVB exposure concomitant with reduced epidermal inflammatory signaling and reduced markers of DNA damage. In the context of aging, old *M. musculus* animals exhibit typical hallmarks including epidermal thinning, increased inflammatory signaling and senescence. However, these age-related changes are absent in old *A. cahirinus* skin. Overall, we find that *A. cahirinus* have evolved novel responses to skin damage that reveals new aspects of its regenerative phenotype.

Introduction

The maintenance and repair of the skin barrier are essential to prevent infection and protect the body from external hazards. However, normal stress and damage during an organism's lifespan deteriorate skin structure and repair through undefined mechanisms. The skin epidermis is composed primarily of keratinocytes derived from basal stem cells that continually renew the differentiated spinous, granular, and cornified suprabasal layers [1]. Together, these cells protect against environmental insults such as radiation, physical injury, dehydration, and pathogens. A major environmental hazard to the skin is ultraviolet (UV) solar radiation, which induces potentially mutagenic DNA damage if left unrepaired. Severely UV-damaged cells undergo either apoptosis or cell cycle arrest coupled with DNA repair before re-entry into

Abbreviations: BrdU, 5-Bromo-2'-deoxyuridine; CC3, Cleaved caspase-3; Cy5, Cyanine 5; DAPI, 4',6-diamidino-2-phenylindole; DsRed, Red fluorescent protein; GFP, Green fluorescent protein; K10, Keratin 10; K14, Keratin 14; Lor, Loricrin; mJ, Millijoule; PBS, Phosphate buffered saline; TBS, Tris-buffered saline; T-T dimer, Thymine dimer.

the cell cycle such that UV-driven proliferation and differentiation of keratinocytes results in thickening of the epidermis [2]. In contrast, aging of the skin induces cellular senescence, thinning of the epidermis and reduced basal stem cell renewal and proliferation [3].

Long-lived or stress-resistant model organisms permit a better understanding of adaptive mechanisms of tissue homeostasis and repair. For example, the Snell dwarf mouse attains a long lifespan through impaired pituitary hormone signaling and its study has informed our understanding of how organismal physiology and longevity are balanced [4, 5]. The naked mole rat *Heterocephalus glaber* (*H*. *glaber)* has evolved distinctive mechanisms of cancer resistance which may be mediated by their cellular microenvironment and immune system [6–8]. In a similar vein, models of vertebrate regeneration such as salamanders and newts have been used extensively to understand the optimal healing of nervous, muscle and connective tissue [9], but a critical barrier to deriving clinical therapies from this work has been a lack of mammalian models of tissue repair. The recent discovery that spiny mice (*A*. *cahirinus*) can fully regenerate skin and hair following wounding or burn injury [10, 11], a feature not observed in typical strains of mice (*M*. *musculus*), permits the study of novel regenerative mechanisms in mammalian skin tissue. However, it is not known how *A*. *cahirinus* responds to other types of skin stress, including UV-damage and chronological aging.

Here, we examine epidermal responses to acute UVB exposure and chronological aging in the conventional C57Bl/6 *M*. *musculus* strain compared to *A*. *cahirinus*. We find that *A*. *cahirinus* has attenuated pathological hallmarks of UVB exposure and aging in conjunction with distinctive differences in epidermal turnover, senescence and inflammation. These processes may underlie the unique skin regeneration phenotype of *A*. *cahirinus*, and such mechanisms can inform therapeutic strategies to manage skin diseases such as skin cancer and aging.

Materials and methods

Mice

For all studies, C57Bl/6 (*M*. *musculus)* mice were acquired from Jackson Labs (#000664). For the UVB experiments, 5–6 month old male *A*. *cahirinus* animals were shipped from the University of Florida and compared to 3–4 month old male C57Bl/6 mice. *M*. *musculus* were housed 4–5 to a cage in mouse cages while *A*. *cahirinus* were housed 2–3 to a cage in rat cages with a 12h/12h light cycle. Animals were housed at Northeastern University for at least 2 weeks prior to UVB or sham treatments to acclimate. For the aging studies, young, female animals of each species at 3–4 months of age were used and old, female animals (*M*. *musculus*: 2 years of age; *A*. *cahirinus*: 4 years of age) were analyzed. The young and old *M*. *musculus* mice were housed at Northeastern University while the young and old *A*. *cahirinus* animals were housed at the University of Florida and University of Kentucky. For the UVB studies, all animals were sacrificed by cervical dislocation. For the aging studies, animals were euthanized either by cervical dislocation (*M*. *musculus*) or isoflurane overdose (*A*. *cahirinus*). All procedures were performed according to IACUC approved procedures from each institution.

Ultraviolet light exposure

Animals were sedated with intraperitoneal ketamine/xylazine anesthesia (50 mg/kg ketamine; 5 mg/kg xylazine) and shaved with clippers prior to UVB exposure. Animals were exposed to a UVB dose of 200 mJ/cm^2 using a dosimeter calibrated UV instrument (310 nm peak output) (Tyler Research, Alberta, Canada). Full-thickness dorsal skin samples in telogen phase were collected and fixed at 24- and 48-hours after irradiation in addition to sham controls and

paraffin embedded cross-sections were prepared for histologic analysis. BrdU (5-Bromo-2'-doxyuridine, Sigma Aldrich, St. Louis, Missouri, USA) was injected intraperitoneally at 100 mg/kg in sterile PBS 24 hours prior to sacrifice. Animals were euthanized by cervical dislocation.

Histology

Tissues were fixed overnight in 10% neutral buffered formalin and thereafter transferred to 70% ethanol at 4˚C until processing. Tissues were processed using an automated tissue processor (Thermo HistoStar, Kalamazoo, Michigan, USA) and embedded in paraffin wax. A microtome (Leica Biosystems, Buffalo Grove, Illinois, USA) was used to cut 4 μm skin cross-sections, which were allowed to dry overnight before de-waxing and further processing. Heat induced epitope retrieval was performed on de-waxed slides with either citrate or Tris-EDTA buffer prior to immunofluorescence staining. Skin cross-sections were blocked for 30 minutes at room temperature in 5% normal goat serum PBS, which was also the primary antibody diluent, unless the target was a phospho-protein in which case 5% normal goat serum TBS was used. Primary antibodies and their usage were as follows: Keratin 14 (chicken, BioLegend #906004, 1:500, San Diego, California, USA), HMGB1 (rabbit, Abcam #AB79823, 1:250, Cambridge, Massachusetts, USA), Lamin B1 (rabbit, Abcam #AB16048, 1:1000), Keratin 10 (rabbit, BioLegend #905404, 1:500), Loricrin (rabbit, BioLegend #905104, 1:500), BrdU (rat, Abcam #AB6326, 1:200), thymine dimer mouse, Novus #NB600-1141, 1:400, Centennial, Colorado, USA), cleaved caspase-3 (rabbit, Cell Signaling #9661, 1:100, Danvers, Massachusetts, USA), γH2AX (rabbit, Cell Signaling #9718, 1:40), and $pSTAT3^{Y705}$ (Cell Signaling #9145, 1:200). Primary antibody incubations were carried out overnight at 4˚C except Keratin 14, Keratin 10, and Loricrin, which were 2 hours at room temperature. Following either PBS or Tris-buffered saline (TBS) wash, secondary detection antibodies conjugated with either AlexaFluor-647 or AlexaFluor-488 (Invitrogen, Carlsbad, California, USA) were diluted in either PBS or TBS at 1:200 were applied for 30 minutes at room temperature. Mounting media with DAPI (4',6-diamidino-2-phenylindole) used was either ProLong Gold (Invitrogen) or ProLong Diamond (Invitrogen), which were used interchangeably and allowed to cure prior to imaging. For thymine dimer staining, a mouse-on-mouse blocking kit (Vector Labs #BMK-2202, Burlingame, California, USA) was used per the manufacturer's instructions.

Hematoxylin and Eosin staining was performed on 4 um de-waxed sections using standard histology protocols using Gill's Hematoxylin No.1 and Eosin Y (Sigma Aldrich). Colorimetric stained slides were mounted with Permount (Fisher Scientific, Pittsburgh, Philadelphia, USA). All brightfield imaging was done using an inverted EVOS XL (Life Technologies, Carlsbad, California) microscope. All fluorescence imaging was performed on either an Revolve R4 (Echo Labs, San Diego, California, USA) microscope equipped with Olympus UPlanFL 10x/0.30, and UPlanFL 20x/0.50 air objectives using DAPI, FITC, and Cy5 fluorescence channels or an Axio Observer Z1 (Zeiss, White Plains, New York, USA), equipped with Plan Apochromat 5x/0.16, 10x/0.45, and 20x/0.8 air objectives and 40x/1.3 and 63x/1.4 oil objectives using DAPI, GFP, DsRed, and Cy5 fluorescence channels.

Image analysis

All image processing and analysis was conducted using ImageJ FIJI (version 2.0.0-rc-69/1.52i, NIH), Photoshop CC 2019 (version 20.0.4, Adobe), and Illustrator CC 2019 (version 23.0.3, Adobe, San Jose, California, USA). Immunofluorescence images first underwent thresholding over entire image set of all samples from the experiment followed by manual counting of positive cells for at least 3 unique fields from each sample. All epidermal analyses only counted

interfollicular epidermal cells and excluded hair follicles. Nuclear HMGB1 positive cells were those that had overlapping signal with their nuclear DAPI signal. Nuclear pSTAT3^{Y705} positive cells were those that had overlapping signal with their nuclear DAPI signal. Lamin B1 positive cells were those that exhibited perinuclear signal relative to their DAPI signal. Keratin 14, Keratin 10, and Loricrin positive cells were those that had DAPI-associated cytoplasmic signal.

Epidermal thickness measurements were performed on H&E stained intact skin cross-sections as previously described [12] by measuring the orthogonal distance from the basement membrane to the outer edge of the cellular epidermis. We measured at least 5 fields per skin sample and made at least 7 measurements per field to generate $>$ 35 thickness measurements per animal.

Gene expression

RNA was extracted by homogenizing whole skin in TRIzol (Invitrogen) reagent using a bead mill apparatus (MPBio 5G, Irvine, California, USA) followed by column purification (Zymo Direct-zol RNA mini prep, Irvine, California, USA) with on column DNase treatment and subsequent elution. 600 ng of total RNA was then reversed transcribed to cDNA (ABI HC cDNA synthesis kit, Waltham, Massachusetts, USA), diluted 1:30 in ultrapure water and mRNA expression was assessed using qPCR with SYBR chemistry. CDK-interacting protein 1 (*Cdkn1a*) was used as a housekeeping gene and its expression did not significantly differ between species or with UVB treatment. Data was analyzed by the delta Ct (ΔCt) method.

Primers are as follows:

M. musculus Cxcl1-Forward: ACTCAAGAATGGTCGCGAGG; *M. musculus Cxcl1*-Reverse: GTGCCATCAGAGCAGTCTGT. *A. cahirinus Cxcl1*-Forward: CCCATGGTTCGGAAGGTTGT; *A. cahirinus Cxcl1*-Reverse: GTTGTCAGACGCCAGCATTC. *M. musculus Il1b*-Forward: TGCCACCTTTTGACAGTGATG; *M. musculus Il1b*-Reverse: TGATGTGCTGCTGCGAGATT. *A. cahirinus Il1b*-Forward: CTGGGCTCCAGAGACACAAG; *A. cahirinus Il1b*-Reverse: GAACCCCTGCATCAACTCCA. *M. musculus Cdkn1a*-Forward: CGGTGTCAGAGTCTAGGGGA; *M. musculus Cdkn1a*-Reverse: AGGATTGGACATGGTGCCTG. *A. cahirinus Cdkn1a*-Forward: TGCACTCTGGTATCTCACGC; *A. cahirinus Cdkn1a*-Reverse: CAGTCGGCGCTTAGAGTGAT. *M. musculus Notch1*-Forward: AGTGTGACCCAGACCTTGTGA; *M. musculus Notch1*-Reverse: AGTGGCTGGAAAGGGACTTG. *A. cahirinus Notch1*-Forward: GCCAGGATTGAATTCCCCCA; *A. cahirinus Notch1*-Reverse: TAGCACATCTGCACATGCCA. *M. musculus Notch2*-Forward: CCCAAGGACTGCGAGTCAGG; *M. musculus Notch2*-Reverse: GGCAGCGGCAGGAATAGTGA. *A. cahirinus Notch2*-Forward: ACGCTCAACTTTCAGACATGC; *A. cahirinus Notch2*-Reverse: GCAAGGATGTCTAGGCGACA.

Statistical analysis

All data were analyzed in Prism 8.0 (GraphPad, San Diego, California, USA) using a two-way analysis of variance (ANOVA) on either log or square root transformed data with Tukey's HSD post-hoc testing for differences between treatments and species. Statistical significance was set as $p<0.05$.

Results

UV-irradiation induced changes to skin epidermal morphology and epidermal stratification of *M. musculus* and *A. cahirinus*

While *A. cahirinus* can fully regenerate skin wounds and burns without scarring [10, 11], it has not been established how this regenerative ability translates to other types of skin damage.

Since UVB radiation is a common form of epidermal damage [13], we sought to compare the morphological changes between *A*. *cahirinus* and *M*. *musculus* epidermis following an acute dose of UVB known to induce epidermal proliferation and DNA damage in *M*. *musculus* [14]. We first measured the total thickness of the cellular epidermis using hematoxylin and eosin staining. As expected, *M*. *musculus* had a significantly thicker epidermis at 48 hours post-UVB compared to sham or 24 hours (Fig 1A). In contrast, there was no appreciable difference in epidermal thickness in response to UVB in *A*. *cahirinus* at 24 hours ($p = 0.21$) or 48 hours ($p = 0.80$) compared to sham (Fig 1B). To understand the processes underlying this differential response, we examined rates of cell division by analyzing post-UVB epidermal incorporation of the synthetic nucleoside 5-bromo-2'-deoxyuridine (BrdU). During imaging, we noted species specific patterns of BrdU labeling in basal and suprabasal epidermal compartments (Fig 1C). To distinguish these changes, we analyzed patterns of label retention in the two compartments separately. In the basal epidermis, BrdU incorporation was significantly lower in *M*. *musculus* basal epidermis 24 hours after UVB-exposure, and significantly higher at 48 hours following UVB compared to both sham and 24 hours (Fig 1D). In contrast, *A*. *cahirinus* epidermis did not exhibit changes in BrdU incorporation at 24 hours post-exposure but was significantly elevated at 48 hours compared to both the sham and 24 hour groups (Fig 1D). In the suprabasal epidermis, both *M*. *musculus* and *A*. *cahirinus* exhibited greater BrdU incorporation at 48 hours compared to sham, however this UV-induced proliferation was greater in *M*. *musculus* (Fig 1E).

Since stem cell fate decisions control the balance of cell division and upward transport through the suprabasal layers [15], we next stained for keratin 14 (K14) to mark the basal stem/progenitor layer, keratin 10 (K10) to mark the spinous layer, and for the Loricrin (Lor) expressing cornified envelope after UVB in each species. During imaging, we noticed species specific patterns of UVB-induced epidermal differentiation, most notably the unique double-positive $K14^+/K10^+$ suprabasal layer in UVB-exposed *A*. *cahirinus* (Fig 1F). We then measured the thicknesses of each of the labeled basal ($K14^+/K10^-$), double-positive ($K14^+/K10^+$), spinous ($K14^-/K10^+$), and cornified (Lor^+) epidermal layers. Exposure to acute UVB resulted in a significantly thicker $K14^+$ layer in *M*. *musculus* by 48 hours but not in *A*. *cahirinus*. However, a double-positive $K14^+/K10^+$ suprabasal epidermal layer was uniquely evident only in *A*. *cahirinus* at 24 and 48 hours post-UVB (Fig 1G). The thickness of the Lor^+ layer between species was similar at all time points and was not statistically different ($p = 0.0986$) in *A*. *cahirinus* at 48 hours (Fig 1G and S1A Fig). Overall, *A*. *cahirinus* skin exhibits a unique program of epidermal stratification and a reduced proliferation response after UVB exposure. This distinctive pattern of differentiation consists of a transient intermediate layer with both basal and spinous characteristics in response to UVB.

Differences in UV-induced damage and epidermal cell death between *M*. *musculus* and *A*. *cahirinus*

In *M*. *musculus* and humans, differentiation and eventual shedding of skin cells via upward transport through the epithelium serves as a method of eliminating damaged and compromised cells [16]. Since we observed an altered differentiation pattern in *A*. *cahirinus* in response to UVB, we reasoned that this could impact the removal of damaged keratinocytes. We first assessed this by measuring the UVB-induced DNA photoproduct thymine dimer (T-T dimer) in the epidermis (Fig 2A). As expected from this dose of UVB, we found significantly higher thymine dimer positive cells in *M*. *musculus* basal epidermis by 24 hours with a near return to sham levels by 48 hours (Fig 2B), yet in the suprabasal layer thymine dimer levels rose significantly by 24 hours and remained elevated at 48 hours (Fig 2C). In *A*. *cahirinus*,

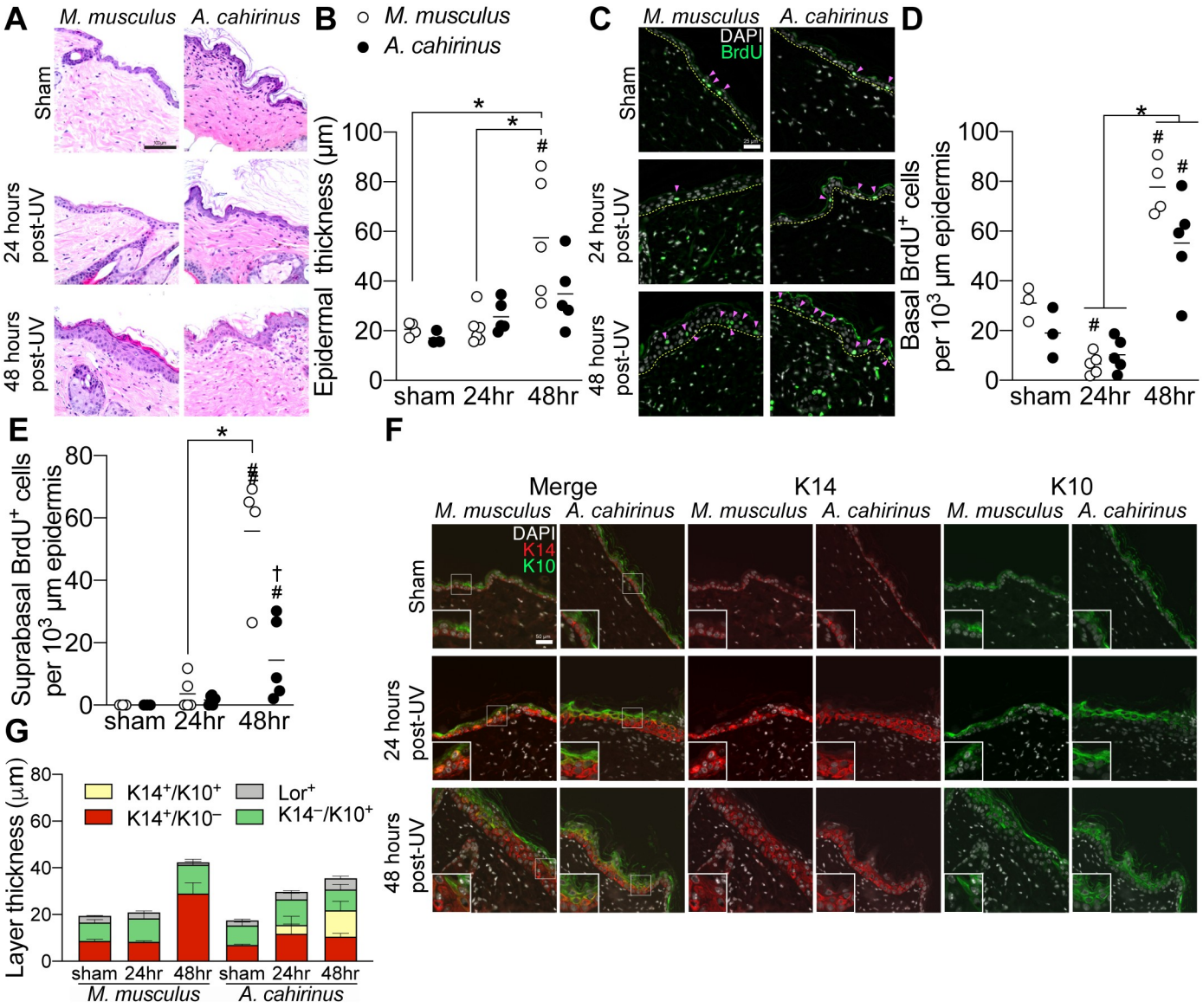

Fig 1. Acute UVB-exposure induces distinctive pattern of skin epidermal differentiation in *A. cahirinus*. *A*, representative brightfield microscopy images of hematoxylin and eosin-stained skin from control (*sham*) and UV-irradiated *M. musculus* and *A. cahirinus*, collected 24 and 48 hours after exposure. Scale bar = 100 μm. *B*, quantification of epidermal thickness. sham of both species, $n = 3$; 24hr *M. musculus*, $n = 6$; 24hr *A. cahirinus*, $n = 5$; 48hr both species, $n = 5$. Thickness was calculated as the distance to the outside of the cellular epidermis orthogonal from the basement membrane within the interfollicular space. *C*, representative immunofluorescence images of epidermal BrdU labeling. The epidermal basement membrane is indicated by the yellow dashed line. Positive cells are indicated by the pink arrows. Scale bar = 25 μm. *D* and *E*, quantification BrdU labeling in (*D*) basal epidermis and (*E*) suprabasal epidermis. sham of both species, $n = 3$; 24hr both species, $n = 5$; 48hr *M. musculus*, $n = 4$; 48hr *A. cahirinus*, $n = 5$. *F*, representative immunofluorescence images of epidermal differentiation markers keratin 14 (*K14*) and keratin 10 (*K10*) labeling with magnified inset of the interface of both labels. Scale bar = 50 μm. *G*, quantification of individual differentiation marker layer thickness. $n = 3$ animals per group. Loricrin images and individual layer comparisons included in S1A–S1E Fig. Data points are biological replicates and lines indicate group means. Bar graphs are mean±SEM. *Significantly different ($p<0.05$) from the indicated group. #Significantly different ($p<0.05$) from species sham control. †Significantly different ($p<0.05$) from *M. musculus* at the same timepoint.

https://doi.org/10.1371/journal.pone.0241617.g001

while we found an induction of thymine dimer positive cells 24 hours following UVB, this UV-response was reduced compared to *M. musculus* animals in both the basal and suprabasal epidermis (Fig 2B and 2C). To extend our thymine dimer results, we next assessed the DNA damage marker γH2AX, which marks repair sites of double strand breaks (Fig 2D). *M. musculus had greater* basal and suprabasal epidermal γH2AX labeling at 24 hours and 48 hours after

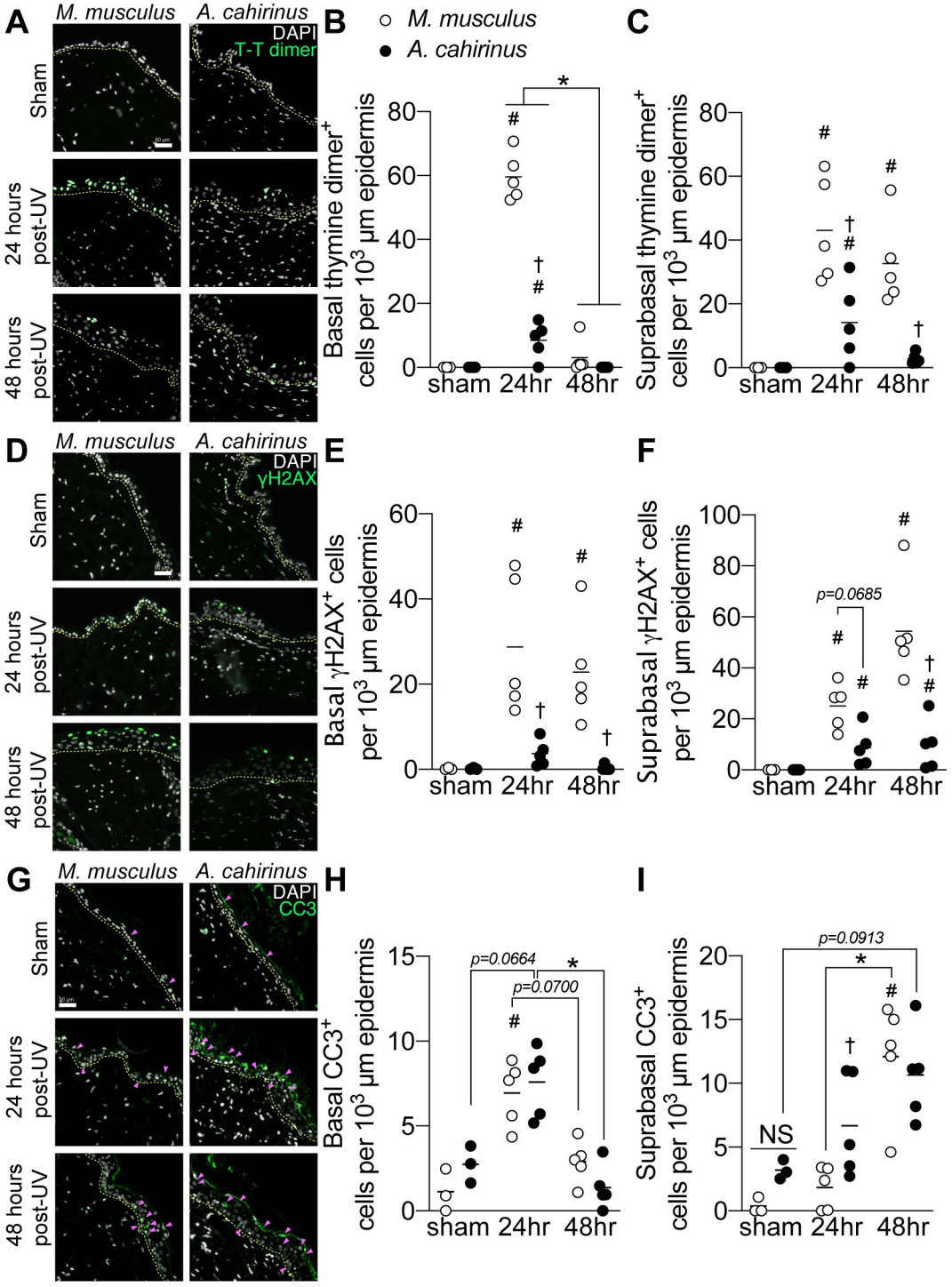

Fig 2. Efficient removal of damaged and dying skin epidermal cells through rapid turnover and apoptosis in acute UVB-exposed *A. cahirinus*. *A*, representative immunofluorescence images of epidermal thymine dimer (*T-T dimer*) labeling of skin from control (*sham*) and UV-irradiated *M. musculus* and *A. cahirinus*, collected 24 and 48 hours after exposure. *B and C*, quantification of thymine dimer labeling in (*B*) basal epidermis and (*C*) suprabasal epidermis. *D*, representative immunofluorescence images of epidermal γH2AX labeling. *E and F*, quantification γH2AX labeling in (*D*) basal epidermis and (*E*) suprabasal epidermis. *G*, representative immunofluorescence images of epidermal cleaved caspase-3 (*CC3)* labeling. Positive cells are indicated by the pink arrows. *H and I*, quantification of cleaved caspase-3 labeling in (*H*) basal and (*I)* suprabasal epidermis. Data points are biological replicates. Lines indicate group means. *Significantly different ($p<0.05$) from the indicated group. #Significantly different ($p<0.05$) relative to sham control. †Significantly different ($p<0.05$) to *M. musculus* at the same timepoint. The epidermal basement membrane is indicated by the yellow dashed line. All scale bars = 50 µm. For all measurements, $n = 3$ sham, $n = 5$ at 24hr and $n = 5$ at 48hr for each species.

https://doi.org/10.1371/journal.pone.0241617.g002

UVB (Fig 2E and 2F). *A. cahirinus* also had more γH2AX-positive cells versus sham at 24 hours in the basal layer, with a similar pattern in the suprabasal layers at 24 and 48 hours (Fig 2E and 2F). However, similar to thymine dimers, there were more γH2AX-positive cells in *M. musculus* compared to *A. cahirinus* at 24 and 48 hours post UVB exposure (Fig 2E and 2F).

To understand the contribution of apoptosis to the post-UVB epidermal response, we measured the abundance of cleaved caspase-3 (CC3) positive cells (Fig 2G). In the basal layer, there was a similar UVB-induced response between species, with an increase in cleaved caspase-3 expressing cells at 24 hours followed by a return to sham levels 48 hours later (Fig 2H). This was in contrast to the suprabasal epidermis, where at 24 hours *A. cahirinus* exhibited a significantly greater number of cleaved caspase-3 expressing cells compared to *M. musculus*. The abundance of suprabasal cleaved caspase-3 expressing cells between species at 48 hours was not significantly different but *M. musculus* levels were significantly elevated at 48 hours *vs* respective sham while *A. cahirinus* levels were not ($p = 0.0913$ for *A. cahirinus vs* sham) (Fig 2I). Thus, *A. cahirinus* epidermis exhibit an earlier and increased induction of suprabasal cell death following UVB exposure compared to *M. musculus*.

Attenuated skin epidermal inflammatory response following UV-irradiation in *A. cahirinus*

Inflammation is a major component of epidermal remodeling following UVB exposure [17]. To gain further insight into the differential UVB responses between *M. musculus* and *A. cahirinus*, we analyzed the epidermal abundance of the damage associated molecular pattern, HMGB1 (Fig 3A). Loss of nuclear HMGB1 is a biomarker of cell stress, senescence, inflammation, and autophagic responses particularly in UVB-exposed basal epidermis [18, 19]. Quantification of HMGB1 labeling revealed that *M. musculus* experiences a significant loss of basal nuclear HMGB1 by 48 hours after UVB (Fig 3B). However, we found that post-UVB *A. cahirinus* basal epidermis retained nuclear HMGB1 labeling similar to sham levels (Fig 3B). Suprabasal levels of HMGB1 were similar between species and treatments (Fig 3C), suggesting that this effect is restricted to basal progenitors. A milieu of pro-inflammatory signaling within the skin also occurs concomitantly to the epidermal hyperplastic response [20]. To better understand the UV-induced inflammatory response in each species, we measured mRNA levels of the inflammation associated genes *Il1b*, *Cxcl1*, *Tgfb1*, *and Mmp9* in whole skin using species specific primers and qPCR. Increased epidermal expression of *Il1b* and *Cxcl1* mediate inflammatory responses after UV-exposure [21], and knockout mouse studies have shown loss of *Tgfb1* and *Mmp9* are associated with increased and prolonged inflammation in the skin epidermis [22, 23]. Acute UVB-irradiation resulted in significant increase in *Cxcl1* in *M. musculus* skin at 48 hours, but levels in *A. cahirinus* were not significantly altered by UVB exposure (Fig 3D). In contrast, *Il1b* expression was not significantly changed by acute UVB-irradiation in either species but was consistently lower in *A. cahirinus* vs. *M. musculus* (Fig 3E). Transcript levels of *Tgf1b* in *M. musculus* skin significantly decreased at 24 hours but *A. cahirinus* levels were unchanged (Fig 3F). Similarly, levels of *Mmp9* in *M. musculus* skin significantly decreased at 24 and 48 hours but *A. cahirinus* levels were not significantly altered by UVB (Fig 3G). Since our stratification marker analysis suggested an altered UV-induced program of terminal differentiation, we also examined molecular processes related to keratinocyte differentiation including nuclear localized STAT3 phosphorylation (Y705) and the expression of Notch pathway molecules. Acute UVB-exposure caused basal epidermal expression of nuclear $pSTAT3^{Y705}$ to trend towards an increase in *M. musculus* at 48 hours ($p = 0.053$), but not at 24 hours compared to sham (S2A and S2B Fig). In contrast, *A. cahirinus* levels were not significantly altered by UVB and trended towards being reduced compared to *M. musculus* at 48

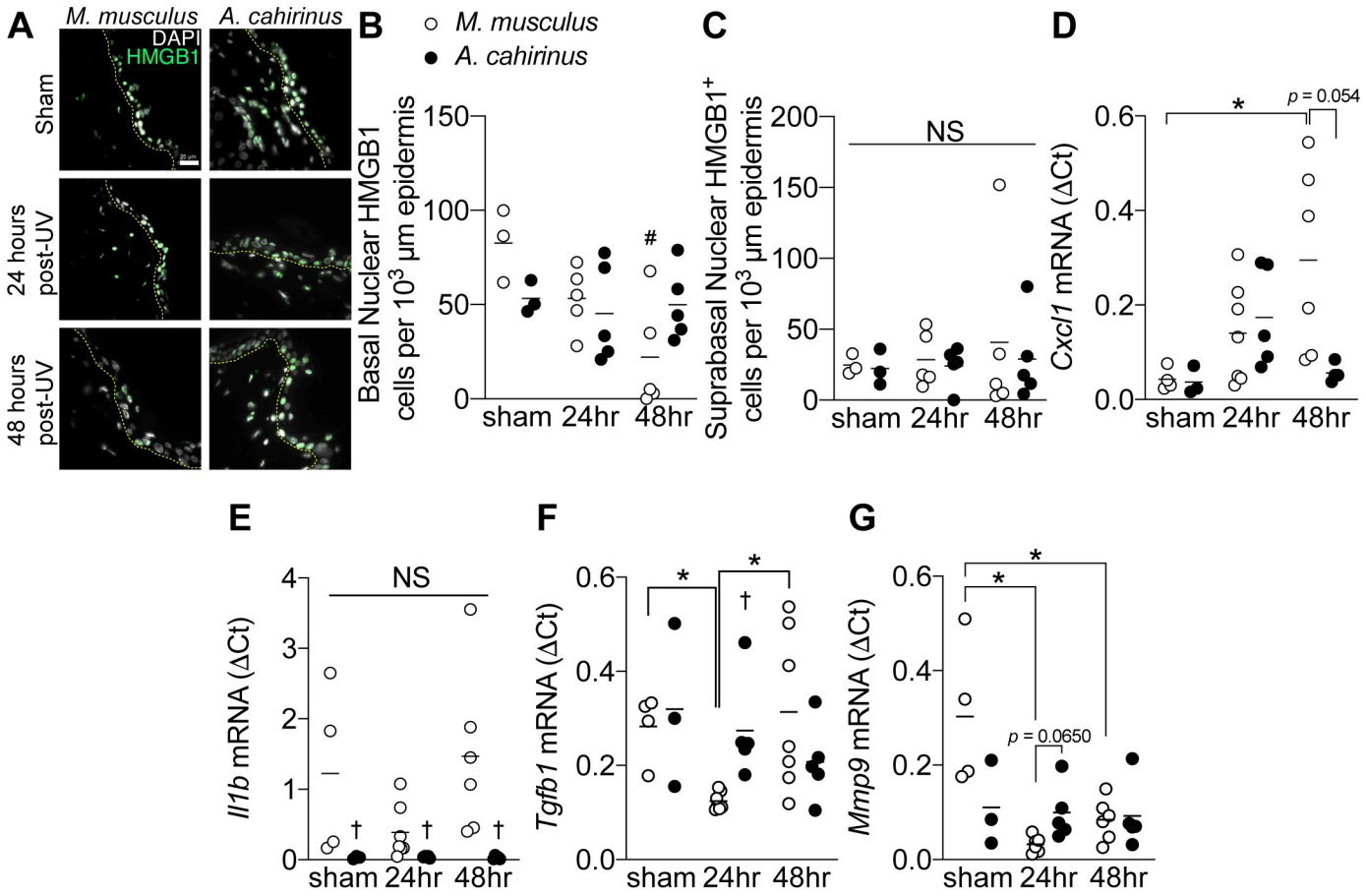

Fig 3. Attenuated skin epidermal inflammatory response following UV-irradiation in *A. cahirinus*. *A*, representative immunofluorescence images of epidermal HMGB1 labeling of skin from control (*sham*) and UV-irradiated *M. musculus* and *A. cahirinus*, collected 24 and 48 hours after exposure. The epidermal basement membrane is indicated by the yellow dashed line. Scale bar = 50 μm. *B* and *C*, quantification of nuclear HMGB1 labeling in (*B*) basal epidermis and (*C*) suprabasal epidermis. *sham*, *n = 3 each species; 24hr and 48hr*, *n = 5 for each species*. *D*, *E*, *F*, *and G*, mRNA expression (ΔCt) of (*D*) *Cxcl1*, (*E*) *Il1b*, (*F*) *Tgfb1*, and (*G*) *Mmp9* in each treatment group as measured by qPCR. For all qPCR: sham, *n* = 3–4 each species; 24hr *n* = 5–7 each species; 48hr *M. musculus*, *n* = 5–6; 48hr *A. cahirinus*, *n* = 3–5 animals per group. Data points are biological replicates and lines indicate group means. *Significantly different ($p<0.05$) from the indicated group. #Significantly different ($p<0.05$) relative to sham control. †Significantly different ($p<0.05$) from *M. musculus* at the same timepoint.

https://doi.org/10.1371/journal.pone.0241617.g003

hours ($p = 0.074$). Additionally, *Notch1* mRNA was elevated overall in *A. cahirinus* vs. *M. musculus* and UVB exposure generally reduced *Notch1* in both species at 24 and 48 hours (S2C Fig). Similarly, *Notch2* mRNA was significantly reduced by UVB at 24 hours only in *M. musculus* and was greater in *A. cahirinus* vs. *M. musculus* at 24 and 48 hours. Overall, compared to *M. musculus*, *A. cahirinus* epidermis resists UVB-driven inflammatory and differentiation-associated changes, consistent with their anti-inflammatory tissue damage response seen after wounding and burn injury [11, 24, 25].

Aging associated epidermal thinning, inflammatory signaling, and senescence are absent in *A. cahirinus*

Total organismal aging is the sum of chronological aging and environmental exposure. We sought to further explore the differences in cellular stress response in these two species by examining their epidermal responses to chronological aging. *A. cahirinus* have a maximal lifespan of 5.9 years, versus 3.5 years in *M. musculus* (C57Bl/6) [26]. Thus, to study aging in these

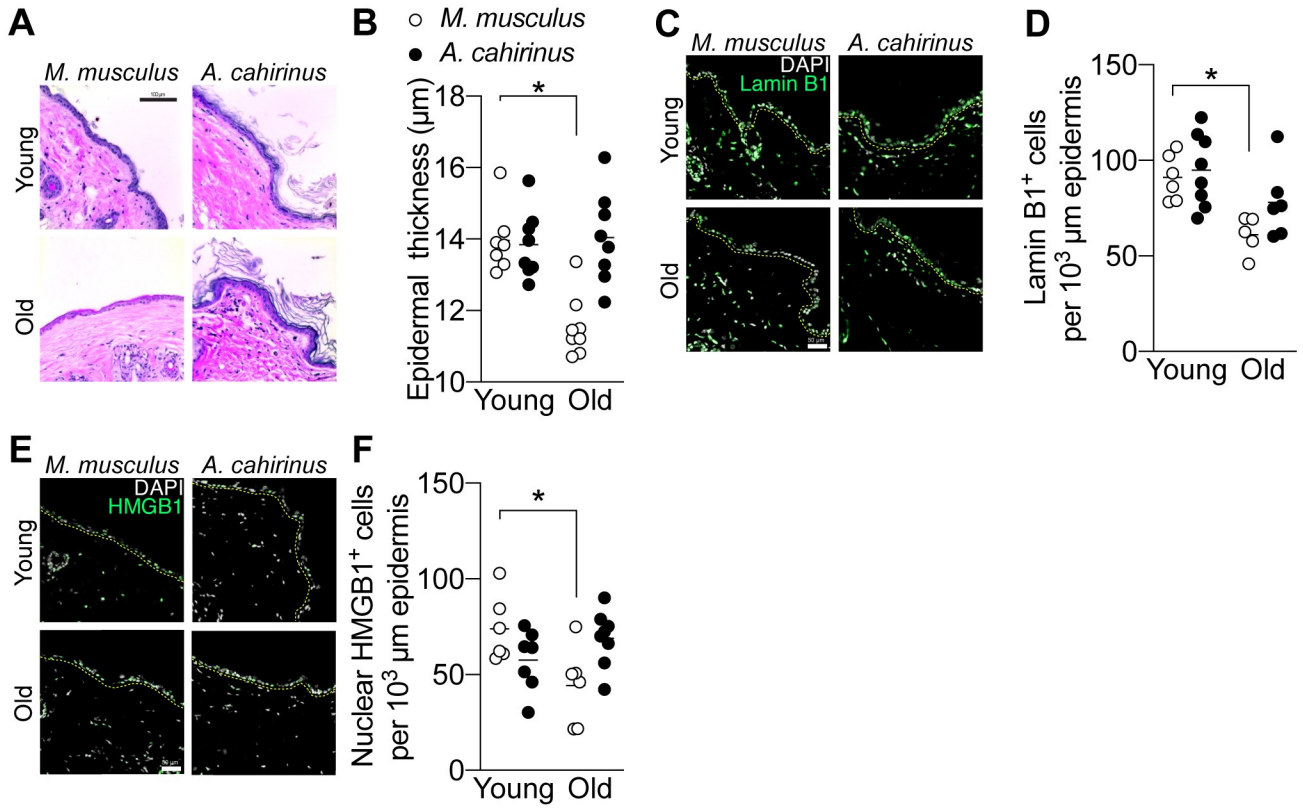

Fig 4. Aging associated epidermal thinning, inflammation, and senescence are absent in *A. cahirinus*. *A*, representative brightfield microscopy images of hematoxylin and eosin-stained intact skin from control (*Young)* and aged (*Old) M. musculus* and *A. cahirinus*. Scale bar = 100 μm. *B*, quantification of epidermal thickness. Thickness was calculated as the distance to the outside of the cellular epidermis orthogonal from the basement membrane within the interfollicular space. *C*, representative immunofluorescence images of epidermal Lamin B1 labeling of skin from each treatment group. Scale bar = 50 μm. $n = 7$ Young and $n = 8$ Old animals of each species. *D*, quantification of epidermal Lamin B1 labeling. $n = 6$ Young *M. musculus;* $n = 8$ Young *A. cahirinus;* $n = 5$ Old *M. musculus*, $n = 6$ Old *A. cahirinus*. *E*, representative immunofluorescence images of epidermal HMGB1 labeling of skin from each treatment group. Scale bar = 50 μm. *F*, quantification of epidermal nuclear HMGB1 labeling. $n = 6$ Young and Old *M. musculus;* $n = 7$ Young and Old *A. cahirinus*. In all immunofluorescent images the epidermal basement membrane is indicated by a yellow dashed line. Data points are biological replicates and lines indicate group means. *Significantly different ($p<0.05$) from the indicated group.

https://doi.org/10.1371/journal.pone.0241617.g004

species, we used young animals from each species at 3–4 months old as well as aged 2-year old *M. musculus* and 4-year old *A. cahirinus* animals. At these ages the species are roughly matched as a fraction of their respective maximum lifespans: approximately 9.4% for young *M. musculus*, 8.4% for young *A. cahirinus*, 56% for old *M. musculus*, and 68% for old *A. cahirinus*. Using formalin fixed skin cross-sections for both species, we used hematoxylin and eosin staining of the skin to reveal morphological changes due to age (Fig 4A). This revealed an expected decrease in the thickness of the cellular epidermis of old versus young *M. musculus* (Fig 4B), however, the cellular epidermal thickness of *A. cahirinus* remained unchanged with age (Fig 4B). To better understand the cellular epidermal thickness differences, we measured the nuclear envelope protein and senescence associated biomarker Lamin B1 (Fig 4C). Similar to previous research by ourselves [27] and others [28, 29], we found a decrease in basal epidermal Lamin B1 with age in *M. musculus* (Fig 4D). However, *A. cahirinus* basal epidermal Lamin B1 labeling was similar to young *M. musculus* and was not different in old *A. cahirinus* versus young (Fig 4D). To corroborate these findings regarding senescence, we also evaluated the proportion of epidermal cells with nuclear HMGB1 staining (Fig 4E). As previously reported by ourselves [27] and others [18], we observed a decrease in epidermal nuclear $HMGB1^+$ cells

with age in *M*. *musculus* (Fig 4F), yet HMGB1 in old *A*. *cahirinus* remained unchanged from young animals (Fig 4F). Collectively, these data show that *A*. *cahirinus* do not exhibit typical hallmarks of epidermal aging at up to 4 years of age.

Discussion

The comparative study of exceptionally long-lived, stress-resistant, or regenerative organisms can be used to provide insight into evolved mechanisms of cellular repair. In this study, we found substantial differences in how the regenerative rodent *A*. *cahirinus* responds to UVB skin damage compared to *M*. *musculus*. This included altered patterns of keratinocyte proliferation and differentiation, an earlier induction of UVB-induced cell death, and an attenuated inflammatory response. The epidermal thickening commonly observed in *M*. *musculus* after UVB was not evident in *A*. *cahirinus* despite similar rates of basal cell proliferation, suggesting an alternative fate of newly formed keratinocytes. Notably, the *A*. *cahirinus* epidermis forms a unique middle suprabasal layer of keratinocytes with both basal and spinous characteristics ($K14^+/K10^+$) which may facilitate increased keratinocyte upward transport and removal. This was supported by the observations of fewer retained damaged cells (thymine dimers, γH2AX) as well as more apoptotic cells transiting the suprabasal epidermis at intermediate stages of repair (24 hours) in *A*. *cahirinus* compared to *M*. *musculus*. Taken together, these data suggest that *A*. *cahirinus skin* epidermis is capable of more rapid removal of damaged and dying cells after UVB-exposure through an enhanced rate of differentiation.

The presence of a co-expressed $K14^+/K10^+$ suprabasal layer in the epidermis has been reported by others, but usually this is observed in skin disorders. For example, in psoriatic human skin biopsies, there is aberrant Notch expression and dual K14/K10 expression [30]. Dysregulated epidermal calcium gradients can also produce dual expression of K14 and K10, such as in the skin blistering disorders Hailey-Hailey disease and Darier disease [31, 32], and in TRPV4 KO mice [33] which suffer defective tight junction formation [34]. Interestingly, TRPV4 is also a nociceptor and those mice had altered pain perception and inflammatory responses after sunburn [33]. Aberrant cell cycle regulation can also cause dual K14/K10 expression as mice lacking epidermal C/EBPβ and C/EBPα exhibit defective cornified envelope formation [35]. In contrast to these pathological examples of K14/K10 co-expression, this suprabasal layer formed after UVB in *A*. *cahirinus* appears to be a physiological skin damage response. Notably, *A*. *cahirinus* executes this distinctive program of epidermal differentiation without marked changes in inflammatory signaling factors (*Cxcl1*, *Il1b*), which is similar to their blunted inflammatory response reported during wound healing [24]. Mechanistically, differences in acute-UVB induced STAT3 and Notch signaling may also explain some of these differences as *A*. *cahirinus* had a did not have significant changes in STAT3 phosphorylation in response to UVB, but sustained a greater expression of *Notch1* and *Notch2*. Mice constitutively expressing STAT3 show an exaggerated hyperplastic response to UV irradiation and while STAT3 deficient mice exhibit reduced stress-induced proliferation [36]. Similarly, loss of keratinocyte Notch1 results in excessive spontaneous differentiation and disruption of the epidermal barrier [37]. The greater Notch expression in *A*. *cahirinus* after UVB exposure may enable co-expression of both basal layer and terminally differentiated markers (K14+/K10+), permitting a more rapid shedding or remodeling of the epidermis after damage.

The study of organisms with long lifespans such as the naked mole rat (*H*. *glaber*) has revealed several unique mechanisms of stress resistance [6, 38]. Long-lived model organisms often also exhibit altered inflammatory and cellular damage responses distinct from humans or laboratory mice which provide cancer resistance or augmented tissue repair [39, 40]. In *H*. *glaber*, cellular senescence is rare, yet cancer rates are very low due to sensitive cellular

growth inhibition, modified tumor suppressor pathways, altered extracellular matrix composition, and a stable epigenome [41]. The evolutionary path to these adaptive differences was likely guided by evolutionary adaptation to the hypoxic subterranean environment of *H. glaber* and the fructose biased metabolism resulting from hypoxia [41]. We reasoned that *A. cahirinus* might have also evolved distinct cellular stress mechanisms to enable extensive tissue regeneration, which parallels the unique survival mechanisms recently found in *A. cahirinus* fibroblasts *in vitro* [42]. We found that *A. cahirinus* epidermis was remarkably resilient to chronological aging stress with minimal changes in epidermal thickness or biomarkers of aging and senescence. It is interesting to note that the MRL/MpJ healer strains of mice also exhibit reduced inflammatory responses to injury and improved recovery outcomes in the corneal epithelium [43] and ear punch wounds [44]. Thus, an attenuated inflammatory response may enable the unique growth and repair patterns of *A. cahirinus* epidermis compared to *M. musculus* and may also explain the differences in biological aging between the species.

Our study of the regenerative African spiny mouse, *A. cahirinus*, has revealed a unique skin response to acute UVB-irradiation which consists of rapid differentiation and apoptosis without prototypical epidermal hyperplasia or inflammation. However, we do not yet understand the precise cellular mechanisms underlying this response. While proliferation and differentiation may be intrinsically regulated, inflammation and clearance of cells is likely related to the altered immunity and inflammation previously reported during skin repair in *A. cahirinus* [11, 45]. Moreover, our findings of improved epidermal tissue repair in *A. cahirinus* extend recent work using models of spinal cord injury [46], ear hole regeneration [47], and muscle damage [48] and suggest that other tissues besides *A. cahirinus* skin may also exhibit attenuated aging pathology. Future work should clarify the molecular underpinnings of improved tissue repair and stress resistance in *A. cahirinus* in order to advance regenerative medicine.

Supporting information

S1 Fig. Acute UVB-exposure induces distinctive pattern of skin epidermal differentiation in *A. cahirinus*. *A*, representative immunofluorescence images of epidermal differentiation markers keratin 14 (*K14*) and loricrin (*Lor*) labeling. *B*, *C*, *D*, *E* individual layer thickness quantification of the *(B)*, $K14^{+}/K10^{-}$ single positive basal layer *(C)*, $K14^{+}/K10^{+}$ double positive middle suprabasal layer *(D)*, $K14^{-}/K10^{-}$ single positive spinous layer and *(E)*, Lor^{+} single positive cornified envelope. $n = 3$ animals per group. Data points are biological replicates and lines indicate group means. *Significantly different ($p<0.05$) from the indicated group.
(TIF)

S2 Fig. Attenuated phospho-STAT3^{Y705} induction after acute UVB-exposure in *A. cahirinus*. *A*, representative immunofluorescence images of epidermal nuclear phosphorylated STAT3 on Y705 ($pSTAT3^{Y705}$) labeling of skin from control (*sham*) and UV-irradiated *M. musculus* and *A. cahirinus*, collected 24 and 48 hours after exposure. Positive cells are indicated by the pink arrows and the epidermal basement membrane is indicated by the yellow dashed line. Scale bar = 50 μm. *B*, quantification of $pSTAT3^{Y705}$ labeling in basal epidermis. $n = 3$ sham of each species; $n = 5$ animals at 24hr and 48hr from each species. *C*, *Notch1* and *D*, *Notch2* mRNA expression in whole skin from UV-irradiated *M. musculus* and *A. cahirinus*, collected from sham controls or 24 and 48 hours after UVB exposure. For all qPCR: sham, $n = 3$–4 each species; *24hr* $n = 5$–7 each species; 48hr *M. musculus*, $n = 5$–6; 48hr *A. cahirinus*, $n = 3$–5 animals per group. All data points are biological replicates and lines indicate group

means. *Significantly different ($p<0.05$) from the indicated group. †Significant ($p<0.05$) overall effect of species.
(TIF)

Acknowledgments

The authors wish to thank E. Crane for assistance with some of the IHC analysis.

Author Contributions

Conceptualization: Wesley Wong, Malcolm Maden, Justin D. Crane.

Data curation: Wesley Wong.

Formal analysis: Wesley Wong, Austin Kim.

Funding acquisition: Justin D. Crane.

Investigation: Wesley Wong, Austin Kim, Justin D. Crane.

Methodology: Wesley Wong.

Resources: James R. Monaghan, Ashley W. Seifert, Malcolm Maden, Justin D. Crane.

Supervision: Justin D. Crane.

Visualization: Wesley Wong.

Writing – original draft: Wesley Wong.

Writing – review & editing: Wesley Wong, Austin Kim, James R. Monaghan, Ashley W. Seifert, Malcolm Maden, Justin D. Crane.

References

1. Fuchs E. Skin stem cells: rising to the surface. J Cell Biol. 2008; 180: 273–284. https://doi.org/10.1083/jcb.200708185 PMID: 18209104
2. El-Abaseri TB, Putta S, Hansen LA. Ultraviolet irradiation induces keratinocyte proliferation and epidermal hyperplasia through the activation of the epidermal growth factor receptor. Carcinogenesis. 2006; 27: 225–231. https://doi.org/10.1093/carcin/bgi220 PMID: 16123117
3. Liu N, Matsumura H, Kato T, Ichinose S, Takada A, Namiki T, et al. Stem cell competition orchestrates skin homeostasis and ageing. Nature. 2019; 568: 344–350. https://doi.org/10.1038/s41586-019-1085-7 PMID: 30944469
4. Flurkey K, Papaconstantinou J, Harrison DE. The Snell dwarf mutation Pit1(dw) can increase life span in mice. Mech Ageing Dev. 2002; 123: 121–130. https://doi.org/10.1016/s0047-6374(01)00339-6 PMID: 11718806
5. Brown-Borg HM. Role of the somatotropic axis in mammalian aging. Handbook of the biology of aging. Elsevier; 2011. pp. 25–45.
6. Seluanov A, Hine C, Azpurua J, Feigenson M, Bozzella M, Mao Z, et al. Hypersensitivity to contact inhibition provides a clue to cancer resistance of naked mole-rat. Proc Natl Acad Sci USA. 2009; 106: 19352–19357. https://doi.org/10.1073/pnas.0905252106 PMID: 19858485
7. Tian X, Azpurua J, Ke Z, Augereau A, Zhang ZD, Vijg J, et al. INK4 locus of the tumor-resistant rodent, the naked mole rat, expresses a functional p15/p16 hybrid isoform. Proc Natl Acad Sci USA. 2015; 112: 1053–1058. https://doi.org/10.1073/pnas.1418203112 PMID: 25550505
8. Hadi F, Kulaberoglu Y, Lazarus K, Beattie P, Smith ESJ, Khaled W. Naked Mole-Rat Cells are Susceptible to Malignant Transformation by SV40LT and Oncogenic Ras. BioRxiv. 2018; https://doi.org/10.1101/404574
9. Joven A, Elewa A, Simon A. Model systems for regeneration: salamanders. Development. 2019; 146. https://doi.org/10.1242/dev.167700 PMID: 31332037

10. Seifert AW, Kiama SG, Seifert MG, Goheen JR, Palmer TM, Maden M. Skin shedding and tissue regeneration in African spiny mice (Acomys). Nature. 2012; 489: 561–565. https://doi.org/10.1038/nature11499 PMID: 23018966

11. Maden M. Optimal skin regeneration after full thickness thermal burn injury in the spiny mouse, Acomys cahirinus. Burns. 2018; 44: 1509–1520. https://doi.org/10.1016/j.burns.2018.05.018 PMID: 29903601

12. Crane JD, MacNeil LG, Lally JS, Ford RJ, Bujak AL, Brar IK, et al. Exercise-stimulated interleukin-15 is controlled by AMPK and regulates skin metabolism and aging. Aging Cell. 2015; 14: 625–634. https://doi.org/10.1111/acel.12341 PMID: 25902870

13. Brash DE, Rudolph JA, Simon JA, Lin A, McKenna GJ, Baden HP, et al. A role for sunlight in skin cancer: UV-induced p53 mutations in squamous cell carcinoma. Proc Natl Acad Sci USA. 1991; 88: 10124–10128. https://doi.org/10.1073/pnas.88.22.10124 PMID: 1946433

14. Trevithick JR, Xiong H, Lee S, Shum DT, Sanford SE, Karlik SJ, et al. Topical tocopherol acetate reduces post-UVB, sunburn-associated erythema, edema, and skin sensitivity in hairless mice. Arch Biochem Biophys. 1992; 296: 575–582. https://doi.org/10.1016/0003-9861(92)90613-2 PMID: 1632644

15. Williams SE, Beronja S, Pasolli HA, Fuchs E. Asymmetric cell divisions promote Notch-dependent epidermal differentiation. Nature. 2011; 470: 353–358. https://doi.org/10.1038/nature09793 PMID: 21331036

16. Freije A, Molinuevo R, Ceballos L, Cagigas M, Alonso-Lecue P, Rodriguez R, et al. Inactivation of p53 in human keratinocytes leads to squamous differentiation and shedding via replication stress and mitotic slippage. Cell Rep. 2014; 9: 1349–1360. https://doi.org/10.1016/j.celrep.2014.10.012 PMID: 25453755

17. Barker JN, Mitra RS, Griffiths CE, Dixit VM, Nickoloff BJ. Keratinocytes as initiators of inflammation. Lancet. 1991; 337: 211–214. https://doi.org/10.1016/0140-6736(91)92168-2 PMID: 1670850

18. Davalos AR, Kawahara M, Malhotra GK, Schaum N, Huang J, Ved U, et al. p53-dependent release of Alarmin HMGB1 is a central mediator of senescent phenotypes. J Cell Biol. 2013; 201: 613–629. https://doi.org/10.1083/jcb.201206006 PMID: 23649808

19. Bald T, Quast T, Landsberg J, Rogava M, Glodde N, Lopez-Ramos D, et al. Ultraviolet-radiation-induced inflammation promotes angiotropism and metastasis in melanoma. Nature. 2014; 507: 109–113. https://doi.org/10.1038/nature13111 PMID: 24572365

20. Ouhtit A, Muller HK, Davis DW, Ullrich SE, McConkey D, Ananthaswamy HN. Temporal events in skin injury and the early adaptive responses in ultraviolet-irradiated mouse skin. Am J Pathol. 2000; 156: 201–207. https://doi.org/10.1016/S0002-9440(10)64720-7 PMID: 10623668

21. Qiang L, Sample A, Shea CR, Soltani K, Macleod KF, He Y-Y. Autophagy gene ATG7 regulates ultraviolet radiation-induced inflammation and skin tumorigenesis. Autophagy. 2017; 13: 2086–2103. https://doi.org/10.1080/15548627.2017.1380757 PMID: 28933598

22. Wang M, Qin X, Mudgett JS, Ferguson TA, Senior RM, Welgus HG. Matrix metalloproteinase deficiencies affect contact hypersensitivity: stromelysin-1 deficiency prevents the response and gelatinase B deficiency prolongs the response. Proc Natl Acad Sci USA. 1999; 96: 6885–6889. https://doi.org/10.1073/pnas.96.12.6885 PMID: 10359808

23. Yoshinaga K, Obata H, Jurukovski V, Mazzieri R, Chen Y, Zilberberg L, et al. Perturbation of transforming growth factor (TGF)-beta1 association with latent TGF-beta binding protein yields inflammation and tumors. Proc Natl Acad Sci USA. 2008; 105: 18758–18763. https://doi.org/10.1073/pnas.0805411105 PMID: 19022904

24. Brant JO, Lopez M-C, Baker HV, Barbazuk WB, Maden M. A Comparative Analysis of Gene Expression Profiles during Skin Regeneration in Mus and Acomys. PLoS One. 2015; 10: e0142931. https://doi.org/10.1371/journal.pone.0142931 PMID: 26606282

25. Gawriluk TR, Simkin J, Hacker CK, Kimani JM, Kiama SG, Ezenwa VO, et al. Mammalian musculoskeletal regeneration is associated with reduced inflammatory cytokines and an influx of T cells. BioRxiv. 2019; https://doi.org/10.1101/723783

26. Edrey YH, Casper D, Huchon D, Mele J, Gelfond JA, Kristan DM, et al. Sustained high levels of neuregulin-1 in the longest-lived rodents; a key determinant of rodent longevity. Aging Cell. 2012; 11: 213–222. https://doi.org/10.1111/j.1474-9726.2011.00772.x PMID: 22103690

27. Wong W, Crane ED, Kuo Y, Kim A, Crane JD. The exercise cytokine interleukin-15 rescues slow wound healing in aged mice. J Biol Chem. 2019; 294: 20024–20038. https://doi.org/10.1074/jbc.RA119.010740 PMID: 31748415

28. Wang AS, Ong PF, Chojnowski A, Clavel C, Dreesen O. Loss of lamin B1 is a biomarker to quantify cellular senescence in photoaged skin. Sci Rep. 2017; 7: 15678. https://doi.org/10.1038/s41598-017-15901-9 PMID: 29142250

29. Freund A, Laberge R-M, Demaria M, Campisi J. Lamin B1 loss is a senescence-associated biomarker. Mol Biol Cell. 2012; 23: 2066–2075. https://doi.org/10.1091/mbc.E11-10-0884 PMID: 22496421

30. Ota T, Takekoshi S, Takagi T, Kitatani K, Toriumi K, Kojima T, et al. Notch signaling may be involved in the abnormal differentiation of epidermal keratinocytes in psoriasis. Acta Histochem Cytochem. 2014; 47: 175–183. https://doi.org/10.1267/ahc.14027 PMID: 25392571

31. Mikkelsen SA, Vangheluwe P, Andersen JP. A Darier disease mutation relieves kinetic constraints imposed by the tail of sarco(endo)plasmic reticulum Ca2+-ATPase 2b. J Biol Chem. 2018; 293: 3880–3889. https://doi.org/10.1074/jbc.RA117.000941 PMID: 29363575

32. Robia SL, Young HS. Skin cells prefer a slower calcium pump. J Biol Chem. 2018; 293: 3890–3891. https://doi.org/10.1074/jbc.H118.002088 PMID: 29667928

33. Moore C, Cevikbas F, Pasolli HA, Chen Y, Kong W, Kempkes C, et al. UVB radiation generates sunburn pain and affects skin by activating epidermal TRPV4 ion channels and triggering endothelin-1 signaling. Proc Natl Acad Sci USA. 2013; 110: E3225–34. https://doi.org/10.1073/pnas.1312933110 PMID: 23929777

34. Sokabe T, Fukumi-Tominaga T, Yonemura S, Mizuno A, Tominaga M. The TRPV4 channel contributes to intercellular junction formation in keratinocytes. J Biol Chem. 2010; 285: 18749–18758. https://doi.org/10.1074/jbc.M110.103606 PMID: 20413591

35. Lopez RG, Garcia-Silva S, Moore SJ, Bereshchenko O, Martinez-Cruz AB, Ermakova O, et al. C/EBPalpha and beta couple interfollicular keratinocyte proliferation arrest to commitment and terminal differentiation. Nat Cell Biol. 2009; 11: 1181–1190. https://doi.org/10.1038/ncb1960 PMID: 19749746

36. Kim DJ, Angel JM, Sano S, DiGiovanni J. Constitutive activation and targeted disruption of signal transducer and activator of transcription 3 (Stat3) in mouse epidermis reveal its critical role in UVB-induced skin carcinogenesis. Oncogene. 2009; 28: 950–960. https://doi.org/10.1038/onc.2008.453 PMID: 19137019

37. Rangarajan A, Talora C, Okuyama R, Nicolas M, Mammucari C, Oh H, et al. Notch signaling is a direct determinant of keratinocyte growth arrest and entry into differentiation. EMBO J. 2001; 20: 3427–3436. https://doi.org/10.1093/emboj/20.13.3427 PMID: 11432830

38. Pérez VI, Buffenstein R, Masamsetti V, Leonard S, Salmon AB, Mele J, et al. Protein stability and resistance to oxidative stress are determinants of longevity in the longest-living rodent, the naked mole-rat. Proc Natl Acad Sci USA. 2009; 106: 3059–3064. https://doi.org/10.1073/pnas.0809620106 PMID: 19223593

39. Eming SA, Hammerschmidt M, Krieg T, Roers A. Interrelation of immunity and tissue repair or regeneration. Semin Cell Dev Biol. 2009; 20: 517–527. https://doi.org/10.1016/j.semcdb.2009.04.009 PMID: 19393325

40. Kowalczyk A, Partha R, Clark NL, Chikina M. Pan-mammalian analysis of molecular constraints underlying extended lifespan. Elife. 2020; 9. https://doi.org/10.7554/eLife.51089 PMID: 32043462

41. Seluanov A, Gladyshev VN, Vijg J, Gorbunova V. Mechanisms of cancer resistance in long-lived mammals. Nat Rev Cancer. 2018; 18: 433–441. https://doi.org/10.1038/s41568-018-0004-9 PMID: 29622806

42. Saxena S, Vekaria H, Sullivan PG, Seifert AW. Connective tissue fibroblasts from highly regenerative mammals are refractory to ROS-induced cellular senescence. Nat Commun. 2019; 10: 4400. https://doi.org/10.1038/s41467-019-12398-w PMID: 31562333

43. Ueno M, Lyons BL, Burzenski LM, Gott B, Shaffer DJ, Roopenian DC, et al. Accelerated wound healing of alkali-burned corneas in MRL mice is associated with a reduced inflammatory signature. Invest Ophthalmol Vis Sci. 2005; 46: 4097–4106. https://doi.org/10.1167/iovs.05-0548 PMID: 16249486

44. Kench JA, Russell DM, Fadok VA, Young SK, Worthen GS, Jones-Carson J, et al. Aberrant Wound Healing and TGF-β Production in the Autoimmune-Prone MRL/+ Mouse. Clin Immunol. 1999; 92: 300–310. https://doi.org/10.1006/clim.1999.4754

45. Simkin J, Gawriluk TR, Gensel JC, Seifert AW. Macrophages are necessary for epimorphic regeneration in African spiny mice. Elife. 2017; 6. https://doi.org/10.7554/eLife.24623 PMID: 28508748

46. Streeter KA, Sunshine MD, Brant JO, Sandoval AGW, Maden M, Fuller DD. Molecular and histologic outcomes following spinal cord injury in spiny mice, Acomys cahirinus. J Comp Neurol. 2019; https://doi.org/10.1002/cne.24836 PMID: 31820438

47. Gawriluk TR, Simkin J, Thompson KL, Biswas SK, Clare-Salzler Z, Kimani JM, et al. Comparative analysis of ear-hole closure identifies epimorphic regeneration as a discrete trait in mammals. Nat Commun. 2016; 7: 11164. https://doi.org/10.1038/ncomms11164 PMID: 27109826

48. Maden M, Brant JO, Rubiano A, Sandoval AGW, Simmons C, Mitchell R, et al. Perfect chronic skeletal muscle regeneration in adult spiny mice, Acomys cahirinus. Sci Rep. 2018; 8: 8920. https://doi.org/10.1038/s41598-018-27178-7 PMID: 29892004